

# IHF-Harmony: Multi-Modality Magnetic Resonance Images Harmonization using Invertible Hierarchy Flow Model

Pengli Zhu<sup>1</sup>, Yitao Zhu<sup>1</sup>, Haowen Pang<sup>1,2</sup>, and Anqi Qiu<sup>1,3,4</sup> (✉)

<sup>1</sup> Department of Health Technology and Informatics, The Hong Kong Polytechnic University, Hong Kong

<sup>2</sup> School of Integrated Circuits and Electronics, Beijing Institute of Technology, China

<sup>3</sup> Mental Health Research Center, The Hong Kong Polytechnic University, Hong Kong  
an-qi.qiu@polyu.edu.hk

<sup>4</sup> Department of Biomedical Engineering, Johns Hopkins University, USA

**Abstract.** Retrospective MRI harmonization is limited by poor scalability across modalities and reliance on traveling subject datasets. To address these challenges, we introduce **IHF-Harmony**, a unified invertible hierarchy flow framework for *multi-modality* harmonization *using unpaired data*. By decomposing the translation process into reversible feature transformations, IHF-Harmony guarantees bijective mapping and lossless reconstruction to *prevent anatomical distortion*. Specifically, an invertible hierarchy flow (IHF) performs hierarchical subtractive coupling to progressively remove artefact-related features, while an artefact-aware normalization (AAN) employs anatomy-fixed feature modulation to accurately transfer target characteristics. Combined with anatomy and artefact consistency loss objectives, IHF-Harmony achieves high-fidelity harmonization that retains source anatomy. Experiments across multiple MRI modalities demonstrate that IHF-Harmony outperforms existing methods in both anatomical fidelity and downstream task performance, facilitating robust harmonization for large-scale multi-site imaging studies. Code will be released upon acceptance.

**Keywords:** Brain MRI · Harmonization · Hierarchy Flow Model.

## 1 Introduction

Magnetic resonance imaging (MRI) is a non-invasive imaging modality that provides exceptional soft-tissue contrast and is widely used for clinical diagnosis, prognosis, and treatment monitoring [22, 21]. Due to the high cost and lengthy acquisition time of MRI, large-scale neuroimaging studies increasingly rely on multi-site data collection to achieve adequate sample sizes and population diversity. However, aggregating data acquired from different scanners and imaging protocols inevitably introduces site-related, non-biological variability, which can confound downstream analyses and obscure subtle biological effects. Therefore, a key requirement for multi-site MRI studies is to effectively mitigate site-specific artefacts while preserving underlying anatomical structures.

Prospective harmonization attempts to reduce inter-site variability by standardizing acquisition protocols across imaging centers, but it requires extensive pilot studies, must be implemented prior to data collection, and is inapplicable to previously acquired datasets. Moreover, residual variability often persists even under harmonized protocols due to inherent differences in scanner hardware and system characteristics [12]. Consequently, retrospective harmonization has emerged as the preferred alternative, enabling post-acquisition correction of existing datasets and improving the reliability of downstream analyses [20].

Existing retrospective harmonization methods can be broadly categorized into statistics-based and learning-based approaches. Statistics-based methods, including intensity normalization [13, 6] and batch-effect correction [5, 4], primarily operate on global intensity distributions or pre-extracted features and are limited in their ability to model spatially varying, anatomy-dependent artefacts. Learning-based methods aim to overcome this limitation by learning nonlinear mappings between imaging sites using machine learning or deep learning models [11, 2, 19, 1]. However, supervised learning approaches typically rely on paired scans from traveling subject datasets, which are rarely available in large-scale or longitudinal studies. Unsupervised deep learning methods alleviate this requirement by learning mappings from unpaired data [9, 10, 18, 17], but most existing approaches focus on site translation between single-modality image pairs, resulting in poor scalability as the number of modalities increases and often failing to sufficiently preserve fine-grained anatomical structures.

To address the above limitations, we propose IHF-Harmony, a unified retrospective harmonization method. Unlike existing approaches, IHF-Harmony harmonizes *multi-modality* MRI using a single deep learning model trained on *unpaired data*. It effectively preserves anatomy by decomposing the translation into reversible feature transformations, which separate anatomical information from artefact-specific features. Our main contributions are outlined as follows:

1. We propose IHF-Harmony, an invertible flow-based framework for *multi-modality* MRI harmonization that jointly models anatomy and artefacts within a single network. By formulating harmonization as bijective feature transformations, the method enables *lossless reconstruction* and consistent *anatomy preservation* while supporting scalable multi-modality translation.
2. An invertible hierarchical flow with subtractive coupling is introduced to progressively disentangle artefact-related features while preserving anatomy. This bijective formulation guarantees *accurate reconstruction* and preserves *fine-grained structures* that are often lost in unsupervised methods.
3. We develop artefact-aware normalization, which applies anatomy-preserving transformations using learnable anatomy-guided affine parameters jointly inferred from source anatomy and target artefacts, allowing images to *maintain structural identity* while *adopting target artefact characteristics*.
4. A comprehensive set of consistency losses is formulated to explicitly enforce *structural fidelity* and *realistic artefact translation*, ensuring robust performance across heterogeneous imaging protocols.

## 2 Methodology

### 2.1 Overall Architecture

Fig. 1 illustrates the IHF-Harmony framework. To explicitly disentangle anatomical structure from site-specific effects, the architecture comprises squeeze operations, invertible hierarchy flows (IHF), and artefact-aware normalization (AAN). A fixed VGG encoder  $E_{\text{vgg}}$  is employed for feature extraction and loss computation. Leveraging its invertible design to prevent information loss, IHF-Harmony defines a forward pass  $E$  and a backward mapping  $E^{-1}$ . Given a source image  $\mathbf{x}$  and a target image  $\mathbf{y}$ , the forward pass maps  $\mathbf{x}$  to latent features  $\mathbf{z}$ , while  $E_{\text{vgg}}$  extracts artefact statistics  $(\mu, \sigma)$  from  $\mathbf{y}$ . Conditioned on  $(\mu, \sigma)$ , the AAN module transforms  $\mathbf{z}$  into  $\hat{\mathbf{z}}$  in the target artefact space. The backward pass subsequently reconstructs the harmonized image  $\hat{\mathbf{x}} = E^{-1}(\hat{\mathbf{z}})$ , preserving the anatomy of  $\mathbf{x}$  while adopting the artefact characteristics of  $\mathbf{y}$ . Detailed descriptions of each component and the training strategy are provided in subsequent sections.

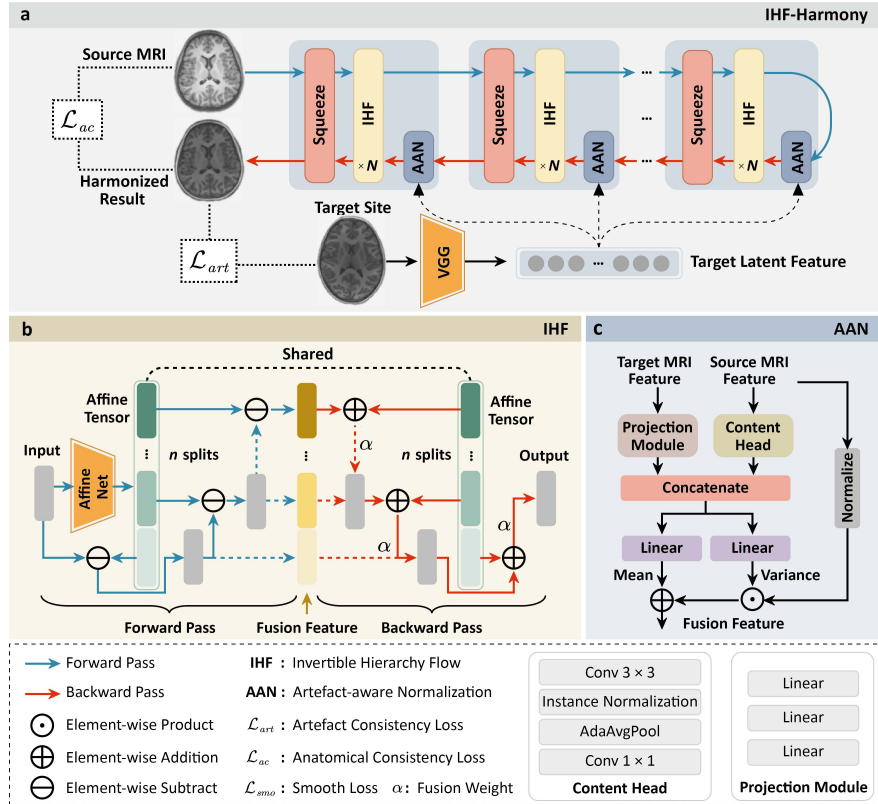


**Fig. 1. Overview of IHF-Harmony.** **a**, IHF-Harmony works in an invertible manner. The blue arrows indicate the forward pass for feature extraction, while the red arrows denote the backward pass for image reconstruction. **b**, invertible hierarchy flow (IHF) performs hierarchical channel-wise subtraction to enable learnable spatial feature transformation and multi-scale fusion. **c**, artefact-aware normalization (AAN) aligns source feature statistics to the target template using anatomy-guided affine parameters.

## 2.2 Squeeze Operation

To reorganize features between consecutive blocks, we adopt a squeeze operation as depicted in Fig. 1a. This mechanism reduces spatial resolution by splitting the input feature into non-overlapping patches and concatenating them along the channel dimension. By compacting spatial information into channel representations, this design facilitates efficient feature interaction in subsequent modules.

## 2.3 Artefact-Aware Normalization

To perform *artefact-aware feature harmonization*, we first extract artefact features from the target image as illustrated in Fig. 1a, where IHF-Harmony decouples anatomical content into normalized features defined by a channel-wise mean  $\mu$  and variance  $\sigma$ . The target artefact embedding  $\mathbf{z}_s$  is formed by concatenating multi-scale statistics extracted from a pre-trained VGG encoder  $\phi$ :

$$\mathbf{z}_s = \text{Concat} [\mu(\phi_1(\mathbf{y})), \dots, \mu(\phi_4(\mathbf{y})), \sigma(\phi_1(\mathbf{y})), \dots, \sigma(\phi_4(\mathbf{y}))], \quad (1)$$

where  $\phi_{1-4}$  denote features from *relu1\_1* to *relu4\_1* layers, and  $\text{Concat}[\cdot]$  represents channel-wise concatenation. As depicted in Fig. 1c, the proposed artefact-aware normalization (AAN) processes target features via a projection module and source anatomy via a content head. These representations are concatenated and fed into parallel linear networks that predict anatomy-guided affine parameters  $\text{AGA}_\sigma$  and  $\text{AGA}_\mu$ , conditioned on both source anatomy  $\mathbf{z}$  and target artefact  $\mathbf{z}_s$ . The resulting harmonized feature  $\hat{\mathbf{z}}$  is formulated as:

$$\hat{\mathbf{z}} = \text{AAN}(\mathbf{z}, \mathbf{z}_s) = \frac{\mathbf{z} - \mu(\mathbf{z})}{\sigma(\mathbf{z})} \cdot \text{AGA}(\mathbf{z}, \mathbf{z}_s)_\sigma + \text{AGA}(\mathbf{z}, \mathbf{z}_s)_\mu. \quad (2)$$

## 2.4 Invertible Hierarchy Flow (IHF)

To achieve *anatomy-preserving* harmonization with enhanced *spatial fusion*, we propose an invertible hierarchy flow (IHF) via hierarchical channel-wise coupling (Fig. 1b). The IHF operates in two stages: a subtractive forward pass for feature encoding, and an additive reverse pass for accurate reconstruction.

**Forward Pass:** Given an unharmonized image  $\mathbf{x}$ , we feed  $\mathbf{x}$  into an affine-net to generate an affine tensor  $\mathbf{a}$  with  $n$ -times expanded channel dimension, which is then split into  $n$  channel-wise components  $\{\mathbf{a}_i\}_{i=1}^n$ . Based on these components, a hierarchical subtractive coupling is applied iteratively. Specifically, the first intermediate feature map is computed as  $\mathbf{h}_1 = \mathbf{x} - \mathbf{a}_1$ , and each subsequent feature map is obtained by subtracting the corresponding affine component from the previous one, i.e.,  $\mathbf{h}_i = \mathbf{h}_{i-1} - \mathbf{a}_i$  for  $i = 2, \dots, n$ . Finally, the output representation  $\mathbf{z}$  is formed by concatenating  $\{\mathbf{h}_i\}_{i=1}^n$  along the channel dimension.

**Reversed Pass:** To reconstruct the harmonized image, we perform an additive coupling in  $n$  steps conditioned on the affine components. Given the latent representation  $\mathbf{z}$ , we normalize it using AAN with artefact-related statistics  $\mu$  and  $\sigma$ , yielding the transformed tensor  $\mathbf{b}$ , which is similarly split into  $n$  channel-wise

components  $\{\mathbf{b}_i\}_{i=1}^n$ . Starting from the last split, the intermediate feature map is computed as  $\mathbf{h}_n = \mathbf{a}_n + \mathbf{b}_n$ . The remaining feature maps are recovered in a recursive manner by fusing the current split with the subsequent intermediate feature map, formulated as  $\mathbf{h}_i = \alpha \cdot (\mathbf{a}_i + \mathbf{b}_i) + (1 - \alpha) \cdot \mathbf{h}_{i+1}$  for  $i = n - 1, \dots, 1$ , where  $\alpha$  is a learnable fusion weight that adaptively balances the contribution of each split. The final harmonized image  $\hat{\mathbf{x}}$  is obtained as the output term  $\mathbf{h}_1$ .

## 2.5 Loss Functions

**Anatomical Consistency Loss.** To preserve underlying anatomy, we adopt a spatially-correlative loss [23] based on feature self-similarity. We extract features using a pre-trained VGG network and calculate the correlation map  $G_{ac}$  as:

$$\mathcal{L}_{ac} = \|G_{ac}(\mathbf{x}) - G_{ac}(\hat{\mathbf{x}})\|_1, \quad (3)$$

where  $G_{ac}(\mathbf{x}) = (f_{\mathbf{x}})^T(f_{\mathbf{x}})$ . Here,  $f_{\mathbf{x}} \in \mathbb{R}^{C \times N_p}$  represents the feature tensor of a patch with  $N_p$  points and  $C$  channels. This mechanism explicitly constrains the model to maintain structural consistency via point-wise correlations.

**Artefact Consistency Loss.** To address semantic misalignment that causes transfer fails in unpaired harmonization, we propose an artefact consistency loss [3] that selectively matches feature distributions via channel-wise filtering. Let  $\phi_i(\cdot)$  denote the  $i$ -th VGG layer ( $i \in \{relu1\_1, 2\_1, 3\_1\}$ ), we compute channel-wise discrepancy as  $D = \|\mu(\phi_i(\hat{\mathbf{x}})) - \mu(\phi_i(\mathbf{y}))\|_2$ , where  $\mu$  denotes channel mean. Let  $C$  index the  $k \cdot N$  channels with smallest  $D$  values, where  $k$  is the selection ratio and  $N$  is the total number of channels. The loss is defined as:

$$\mathcal{L}_{art} = \sum_i \sum_{j \in C} (\|\mu(\phi_{i,j}(\hat{\mathbf{x}})) - \mu(\phi_{i,j}(\mathbf{y}))\|_2 + \|s(\phi_{i,j}(\hat{\mathbf{x}})) - s(\phi_{i,j}(\mathbf{y}))\|_2), \quad (4)$$

where  $s$  denotes the channel standard deviation, and  $k$  is empirically set to 0.9 to align artefact statistics while handling anatomical variations in unpaired data.

**Overall Objective.** The final objective is a weighted sum of the above losses:

$$\mathcal{L}_{total} = \lambda_{ac}\mathcal{L}_{ac} + \lambda_{art}\mathcal{L}_{art}, \quad (5)$$

where  $\lambda_{ac}$  and  $\lambda_{art}$  are weights balancing image fidelity and harmonized intensity.

## 2.6 Implementation

**Dataset** We evaluated IHF-Harmony on the Adolescent Brain Cognitive Development (ABCD) study<sup>1</sup>[7], comprising multi-vendor T1, T2, and diffusion-weighted MRI. For each modality, we allocated 200 volumes per vendor for training, with approximately 2,000 volumes reserved for validation and testing. To further assess cross-site harmonization, we utilized two traveling subject datasets: SRPBS-TS[15] for structural MRI and HDD[16] for diffusion MRI, allocating 5 volumes per site for training and the remainder for evaluation. All traveling images were registered to a common space prior to harmonization.

<sup>1</sup> <https://abcdstudy.org/>

**Optimization** IHF-Harmony was implemented in PyTorch 1.13.1 and evaluated on an NVIDIA Tesla A100 GPU. To leverage volumetric context and ensure spatial smoothness, we adopted a 2.5D training strategy where each slice is stacked with two adjacent neighbors to form a three-channel input, with intensities normalized to  $[-1, 1]$ . We employed the ADAM optimizer[8] with a learning rate of  $1 \times 10^{-4}$  and a batch size of 32. The loss weights were set to  $\lambda_{ac} = 1$  and  $\lambda_{art} = 2$  across all datasets, and the training was conducted for 300 epochs.

### 3 Experimental Results

#### 3.1 Removal of Vendor Variance with Image Fidelity Preservation

We evaluated the multi-vendor harmonization performance of IHF-Harmony across three MRI modalities utilizing the ABCD study [7], with visualized results presented in Fig. 2. For each panel, the first column displays the source images, while the subsequent columns present the harmonized outputs corresponding to GE, Philips, and Siemens targets, respectively. Qualitative assessment demonstrates that IHF-Harmony effectively adapts contrast and preserves anatomical details, thereby ensuring high image fidelity. Notably, when the source and target vendors are identical, IHF-Harmony maintains both the original contrast and anatomical integrity, highlighting its robustness against over-correction.

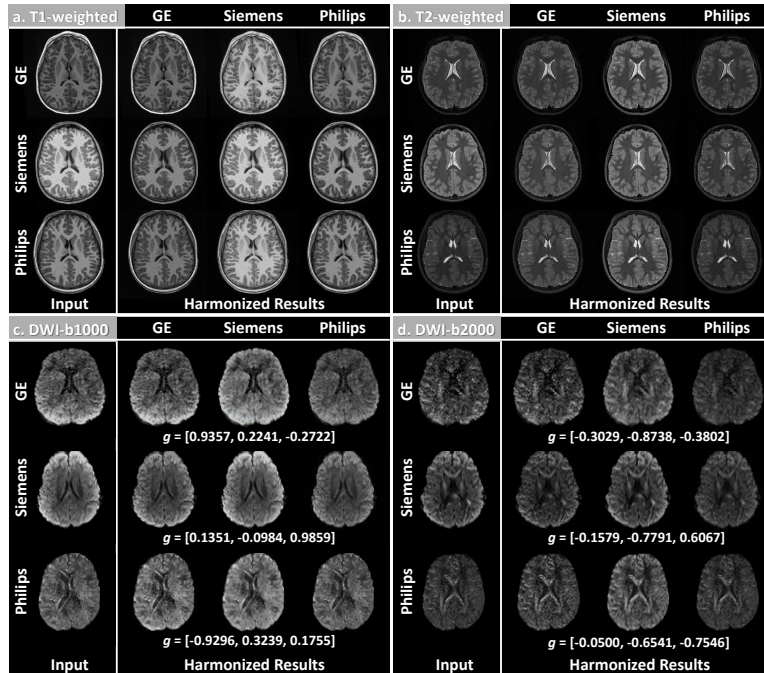


**Fig. 2. Multi-modality MRI harmonization across vendors.** Representative results for **a**, T1-weighted images, **b**, T2-weighted images, and **c–d**, diffusion-weighted images. The leftmost column displays original unharmonized images, followed by results harmonized to GE, Siemens, and Philips scanners, respectively.

### 3.2 Structural MRI Harmonization and Histogram Consistency

We further evaluated IHF-Harmony on structural MRI using the SRPBS-TS dataset [15], designating the COI site as the target domain. Comparisons were conducted against two non-learning baselines, including histogram matching (HM) [13] and spectrum swapping-based image-level harmonization (SSIMH) [6], as well as two learning-based approaches, i.e., conditional GAN (cGAN) [11] and Site Mix (SiMix) [19]. As shown in Fig. 3c, IHF-Harmony outperforms all comparative methods across multiple metrics, including RMSE, MS-SSIM, LPIPS and PSNR, indicating superior contrast harmonization and anatomical detail preservation. The visual results in Fig. 3a further show more consistent intensity profiles across sites while maintaining structural integrity. Additionally, we assessed intensity distribution consistency using kernel density estimation (KDE) [14]. As illustrated in Fig. 3b, the raw images exhibit pronounced, site-related intensity shifts, whereas IHF-Harmony effectively aligns the intensity distributions of all nine source sites with that of the target domain.

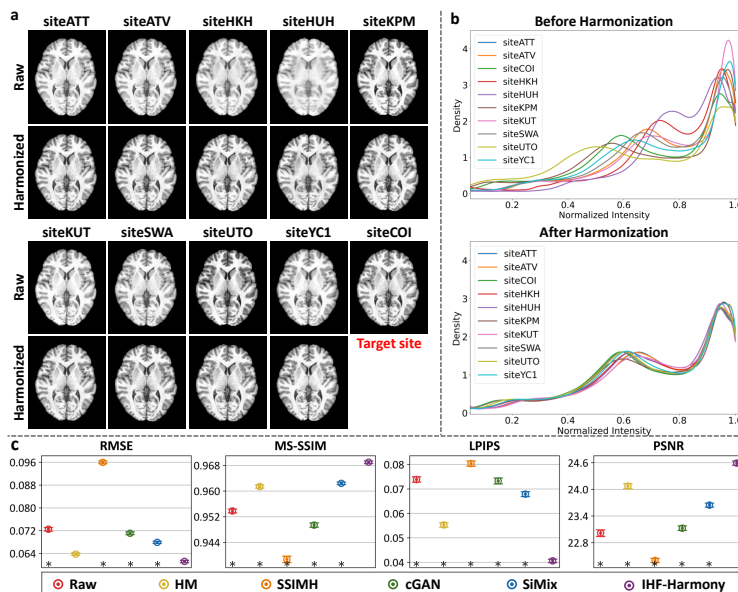


**Fig. 3. Numerical evaluation of harmonization outcomes in structural MRI.** a–b, visual inspection and histogram distribution comparison for multi-site harmonization. c, quantitative comparison of different harmonization methods. Multiple metrics were used for evaluation ( $*p < 0.0001$ , two-sided  $t$ -test) and mean values are marked by bullseye symbols and standard errors by error bars.

### 3.3 Diffusion MRI Harmonization and Model Fitting Consistency

We assessed the generalizability of IHF-Harmony on diffusion MRI via the HDD dataset [16] through downstream harmonization tasks, focusing on the consistency of three microstructural parameter maps: fractional anisotropy (FA), neurite density index (NDI), and orientation dispersion index (ODI). As depicted

in Fig. 4, IHF-Harmony preserves complex anatomical structures while effectively mitigating scanner- and channel-induced variability. Quantitative results further demonstrate reduced site-specific bias and improved structural fidelity, confirming the effectiveness in harmonizing multi-site diffusion MRI.

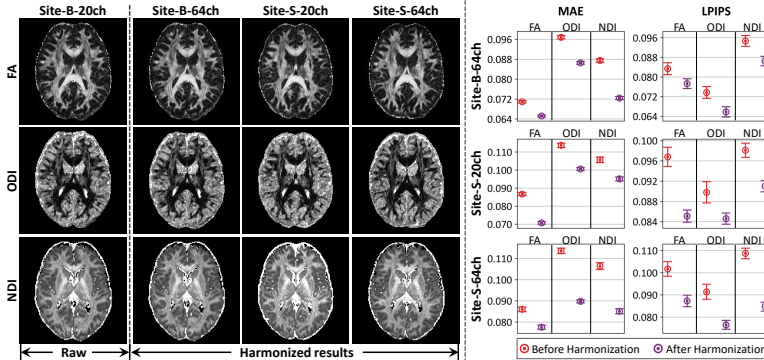


**Fig. 4. Validation of diffusion MRI harmonization via parameter fitting consistency.** The left and right panels show parameter maps used for qualitative and quantitative analysis of scanner- and channel-specific harmonization results, respectively. (B/S: scanner; 20/64ch: channel)

### 3.4 Ablation Studies

To evaluate the contribution of each loss component within IHF-Harmony, we conducted ablation studies on the SRPBS-TS dataset [15] under identical experimental settings. As shown in Table 1, the incremental integration of proposed loss terms leads to consistent improvements across all metrics. The decline in RMSE and LPIPS, coupled with gains in PSNR and MS-SSIM, underscores the necessity of each objective function in improving overall harmonization quality.

**Table 1.** Ablation results of IHF-Harmony with different losses

	RMSE ↓	MS-SSIM ↑	PSNR ↑	LPIPS ↓
w/o $\mathcal{L}_{ac}$ & $\mathcal{L}_{art}$	$0.4196 \pm 0.0012$	$0.5844 \pm 0.0043$	$7.54 \pm 0.026$	$0.4761 \pm 0.0033$
w/o $\mathcal{L}_{art}$	$0.1157 \pm 0.0012$	$0.8844 \pm 0.0012$	$18.75 \pm 0.09$	$0.1416 \pm 0.0014$
w/o $\mathcal{L}_{ac}$	$0.0935 \pm 0.0007$	$0.9079 \pm 0.0011$	$20.58 \pm 0.06$	$0.0570 \pm 0.0009$
<b>Full model</b>	<b><math>0.0612 \pm 0.0004</math></b>	<b><math>0.9690 \pm 0.0004</math></b>	<b><math>24.59 \pm 0.05</math></b>	<b><math>0.0406 \pm 0.0009</math></b>

## 4 Conclusion

This study presents IHF-Harmony, a unified invertible flow-based framework designed to mitigate site-specific artefacts while preserving anatomical structures in multi-modality MRI. By integrating invertible hierarchy flows with artefact-aware normalization, it enables lossless, high-fidelity harmonization using only site-labeled images, without requiring traveling subject datasets. Experiments demonstrate that IHF-Harmony consistently outperforms comparative methods in anatomical preservation and downstream task performance, providing a robust solution for integrating heterogeneous datasets in large-scale clinical studies.

**Acknowledgements.** This research/project is supported by Brain Science and Brain-like Intelligence Technology - National Science and Technology Major Project (2022ZD0209000). Additional support is provided by the University Grants Committee (GRF: 15201124), and the Hong Kong Global STEM Scholar scheme.

**Disclosure of Interests.** The authors have no competing interests to declare that are relevant to the content of this article.

## References

1. Beizae, F., Lodygensky, G.A., Adamson, C.L., Thompson, D.K., Cheong, J.L., Spittle, A.J., Anderson, P.J., Desrosiers, C., Dolz, J.: Harmonizing flows: Leveraging normalizing flows for unsupervised and source-free mri harmonization. *Medical Image Analysis* **101**, 103483 (2025)
2. Cackowski, S., Barbier, E.L., Dojat, M., Christen, T.: Imunity: A generalizable vae-gan solution for multicenter mr image harmonization. *Medical Image Analysis* **88**, 102799 (2023)
3. Fan, W., Chen, J., Liu, Z.: Hierarchy flow for high-fidelity image-to-image translation. *arXiv preprint arXiv:2308.06909* (2023)
4. Fortin, J.P., Cullen, N., Sheline, Y.I., Taylor, W.D., Aselcioglu, I., Cook, P.A., Adams, P., Cooper, C., Fava, M., McGrath, P.J., McInnis, M., Phillips, M.L., Trivedi, M.H., Weissman, M.M., Shinohara, R.T.: Harmonization of cortical thickness measurements across scanners and sites. *NeuroImage* **167**, 104–120 (feb 2018). <https://doi.org/10.1016/j.neuroimage.2017.11.024>
5. Fortin, J.P., Parker, D., Tunç, B., Watanabe, T., Elliott, M.A., Ruparel, K., Roalf, D.R., Satterthwaite, T.D., Gur, R.C., Gur, R.E., Schultz, R.T., Verma, R., Shinohara, R.T.: Harmonization of multi-site diffusion tensor imaging data. *NeuroImage* **161**, 149–170 (nov 2017). <https://doi.org/10.1016/j.neuroimage.2017.08.047>
6. Guan, H., Liu, S., Lin, W., Yap, P.T., Liu, M.: Fast image-level mri harmonization via spectrum analysis. In: *International Workshop on Machine Learning in Medical Imaging*. pp. 201–209. Springer (2022)
7. Jernigan, T.L., Brown, S.A., Dowling, G.J.: The adolescent brain cognitive development study. *Journal of Research on Adolescence* **28**(1), 154–156 (feb 2018). <https://doi.org/10.1111/jora.12374>
8. Kingma, D.P., Ba, J.: Adam: A method for stochastic optimization. *arXiv preprint arXiv:1412.6980* (2014)
9. Liu, M., Maiti, P., Thomopoulos, S., Zhu, A., Chai, Y., Kim, H., Jahanshad, N.: Style transfer using generative adversarial networks for multi-site mri harmonization. In: *International conference on medical image computing and computer-assisted intervention*. pp. 313–322. Springer (2021)
10. Liu, S., Yap, P.T.: Learning multi-site harmonization of magnetic resonance images without traveling human phantoms. *Communications Engineering* **3**(1), 6 (2024)
11. Ravano, V., Démonet, J.F., Damian, D., Meuli, R., Piredda, G.F., Huelnhagen, T., Maréchal, B., Thiran, J.P., Kober, T., Richiardi, J.: Neuroimaging harmonization using cgans: image similarity metrics poorly predict cross-protocol volumetric consistency. In: *International Workshop on Machine Learning in Clinical Neuroimaging*. pp. 83–92. Springer (2022)

12. Shinohara, R., Oh, J., Nair, G., Calabresi, P., Davatzikos, C., Doshi, J., Henry, R., Kim, G., Linn, K., Papinutto, N., Pelletier, D., Pham, D., Reich, D., Rooney, W., Roy, S., Stern, W., Tummala, S., Yousuf, F., Zhu, A., Sicotte, N., and, R.B.: Volumetric analysis from a harmonized multisite brain MRI study of a single subject with multiple sclerosis. *American Journal of Neuroradiology* **38**(8), 1501–1509 (Jun 2017). <https://doi.org/10.3174/ajnr.a5254>
13. Shinohara, R.T., Sweeney, E.M., Goldsmith, J., Shiee, N., Mateen, F.J., Calabresi, P.A., Jarso, S., Pham, D.L., Reich, D.S., Crainiceanu, C.M., et al.: Statistical normalization techniques for magnetic resonance imaging. *NeuroImage: Clinical* **6**, 9–19 (2014)
14. Silverman, B.W.: *Density estimation for statistics and data analysis*. Routledge (2018)
15. Tanaka, S.C., Yamashita, A., Yahata, N., Itahashi, T., Lisi, G., Yamada, T., Ichikawa, N., Takamura, M., Yoshihara, Y., Kunitatsu, A., et al.: A multi-site, multi-disorder resting-state magnetic resonance image database. *Scientific data* **8**(1), 227 (2021)
16. Weninger, L.D., Müller, S., Merhof, D.: Deep learning-based analysis of diffusion mri image data from multicenter studies and from glioma patients. Tech. rep., Lehrstuhl für Bildverarbeitung (2023)
17. Wu, M., Yu, M., Jing, S., Yap, P.T., Zhang, Z., Liu, M.: Unpaired volumetric harmonization of brain mri with conditional latent diffusion. *Medical Image Analysis* **107**, 103849 (2026). <https://doi.org/https://doi.org/10.1016/j.media.2025.103849>
18. Wu, M., Yu, M., Lin, W., Yap, P.T., Liu, M.: Unpaired multi-site brain mri harmonization with image style-guided latent diffusion. In: *International Conference on Medical Image Computing and Computer-Assisted Intervention*. pp. 683–693. Springer (2025)
19. Xu, C., Li, J., Wang, Y., Wang, L., Wang, Y., Zhang, X., Liu, W., Chen, J., Vatian, A., Gusarova, N., et al.: Simix: A domain generalization method for cross-site brain mri harmonization via site mixing. *NeuroImage* **299**, 120812 (2024)
20. Yu, M., Linn, K.A., Cook, P.A., Phillips, M.L., McInnis, M., Fava, M., Trivedi, M.H., Weissman, M.M., Shinohara, R.T., Sheline, Y.I.: Statistical harmonization corrects site effects in functional connectivity measurements from multi-site fMRI data. *Human Brain Mapping* **39**(11), 4213–4227 (jul 2018). <https://doi.org/10.1002/hbm.24241>
21. Zhu, P., Fu, Y., Chen, N., Qiu, A.: Q-space guided collaborative attention translation network for flexible diffusion-weighted images synthesis. In: *International Conference on Medical Image Computing and Computer-Assisted Intervention*. pp. 501–511. Springer (2025)
22. Zhu, P., Fu, Y., Chen, N., Qiu, A.: Q-space guided multi-modal translation network for diffusion-weighted image synthesis. *IEEE Transactions on Medical Imaging* (2025)
23. Zhu, P., Liu, C., Fu, Y., Chen, N., Qiu, A.: Cycle-conditional diffusion model for noise correction of diffusion-weighted images using unpaired data. *Medical image analysis p. 103579* (2025)